ELSEVIER

Thin-Walled Structures 38 (2000) 53–77

THIN-WALLED STRUCTURES

www.elsevier.com/locate/tws

Buckling analysis of skew laminate plates subjected to uniaxial inplane loads

H.-T. Hu *, W.-L. Tzeng

Department of Civil Engineering, National Cheng Kung University, Tainan 701, Taiwan, R.O.C.

Received 1 July 1999; received in revised form 9 May 2000; accepted 18 May 2000

Abstract

Elastic stability of skew composite laminate plates subjected to uniaxial inplane compressive forces has been studied. The critical buckling loads of the skew laminate plates are carried out by the bifurication buckling analysis implemented in finite element program ABAQUS. The effects of skew angles, laminate layups, plate aspect ratios, plate thicknesses, central circular cutouts, and edge conditions on the buckling resistance of skew composite laminate plates are presented.

Keywords: Buckling; Skew laminate plates; Finite elements

1. Introduction

Due to light weight and high strength, the use of fiber-composite laminate materials has been increased rapidly in recent years. The composite laminate plates in service are commonly subjected to compressive forces that may cause buckling. Hence, structural instability becomes a major concern in safe and reliable design of the composite plates. In the literature, most stability studies of fiber-composite laminate plates have been focused on rectangular plates [1–8]. Less attention has been paid to skew laminate plates [9,10]. It is known that the buckling resistance of rectangular composite laminate plates depends on end conditions [4,7], ply orientations [1,2,4,5,7] and geometric variables such as aspect ratios, thicknesses and cutouts [3,4,6–8]. For skew composite plates, in addition to those factors, the plate skew

* Corresponding author. Tel.: +886-6-2757 575 ext 63168; fax: +886-6-2358 542.
E-mail address: hthu@mail.ncku.edu.tw (H.-T. Hu).

0263-8231/00/$ - see front matter
PII: S0263-8231(00)00029-X

angle, α (Fig. 1), should also be a key factor that influences the buckling resistance of the plates [9–12].

In this investigation, buckling analyses of skew composite laminate plates subjected to uniaxial compressive force N (Fig. 1) are performed. The skew angle α of the plates varies from 50° to 90°. The laminate layups of these plates are $[\pm\theta]_{ns}$ ($0°\leq\theta\leq90°$), $[\alpha/0]_{ns}$, $[90/0]_{ns}$ (n=2,10), $[90/45/0/-45]_s$ and $[90/45/0/-45]_{5s}$. The plates in analysis have various laminate layups, different end conditions, different plate aspect ratios, and may contain central circular cutouts. The critical buckling loads N_{cr} of the skew laminate plates are calculated by the bifurcation buckling analysis implemented in the ABAQUS finite element program [13]. Through this study, the effects of skew angles, laminate layups, plate aspect ratios, plate thicknesses, central circular cutouts and end conditions on the buckling resistance of skew composite plates are demonstrated.

2. Bifurcation buckling analysis

In the finite-element analysis, a system of nonlinear algebraic equations results in the incremental form:

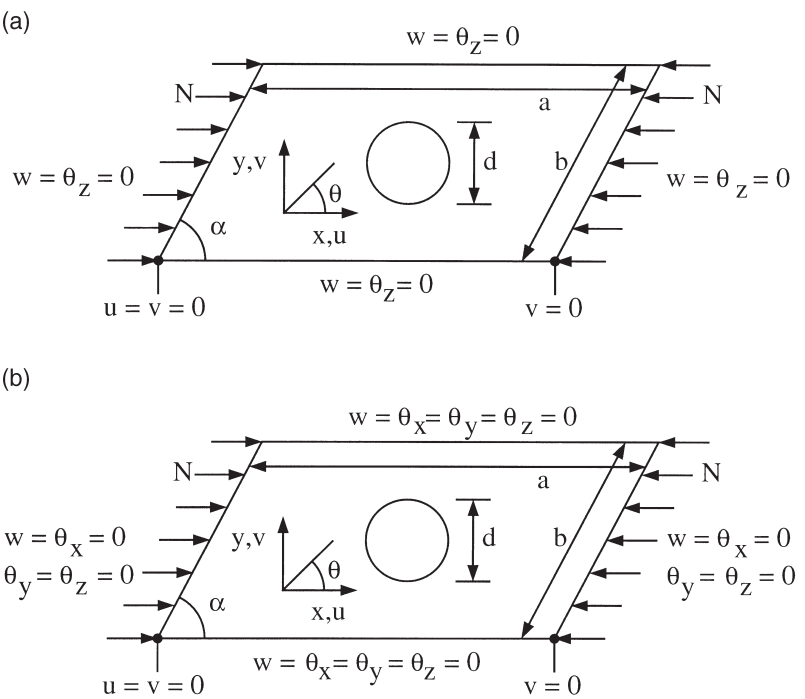

Fig. 1. Skew composite laminate plates with different edge conditions: (a) simply supported edges; (b) fixed edges.

$$[K_t]d\{u\}=d\{p\} \tag{1}$$

where $[K_t]$ is the tangent stiffness matrix, $d\{u\}$ the incremental nodal displacement vector and $d\{p\}$ the incremental nodal force vector.

Within the range of elastic behavior, it is known that when the deformation of a structure is small, the nonlinear theory leads to the same critical load as the linear theory [14]. Consequently, if only the buckling load is to be determined, the calculation can be greatly simplified by assuming the deformation to be small and we can neglect the nonlinear terms which are functions of nodal displacements in the tangent stiffness matrix. The linearized formulation then gives rise to a tangent stiffness matrix in the following expression [15]:

$$[K_t]=[K_L]+[K_\sigma] \tag{2}$$

where $[K_L]$ is a linear stiffness matrix and $[K_\sigma]$ a stress stiffness matrix. If a stress stiffness matrix $[K_\sigma]_{ref}$ is generated according to a reference load $\{p\}_{ref}$, for another load level $\{p\}$ with λ a scalar multiplier, we have

$$\{p\}=\lambda\{p\}_{ref} \tag{3}$$

$$[K_\sigma]=\lambda[K_\sigma]_{ref} \tag{4}$$

When buckling occurs, the external loads do not change, i.e., $d\{p\}=0$. Then the bifurcation solution for the linearized buckling problem may be determined from the following eigenvalue equation:

$$([K_L]+\lambda_{cr}[K_\sigma]_{ref})d\{u\}=\{0\} \tag{5}$$

where λ_{cr} is an eigenvalue and $d\{u\}$ becomes the eigenvector defining the buckling mode. The critical load $\{p\}_{cr}$ can be obtained from $\{p\}_{cr}=\lambda_{cr}\{p\}_{ref}$. In ABAQUS, a subspace iteration procedure [16] is used to solve for the eigenvalues and eigenvectors.

3. Constitutive matrix for fiber-composite laminae

In finite element analysis, the laminate plates are modeled by eight-node isoparametric laminate shell elements with six degrees of freedom per node (three displacements and three rotations). The formulation of the shell element allows transverse shear deformation [13].

During the analysis, the constitutive matrices of composite materials at element integration points must be calculated before the stiffness matrices are assembled from element level to global level. For fiber-composite laminate materials, each lamina can be considered as an orthotropic layer. The stress–strain relations for a lamina in the material coordinates (1,2,3) (Fig. 2) at an element integration point can be written as

$$\{\sigma'\}=[Q_1']\{\varepsilon'\} \tag{6}$$

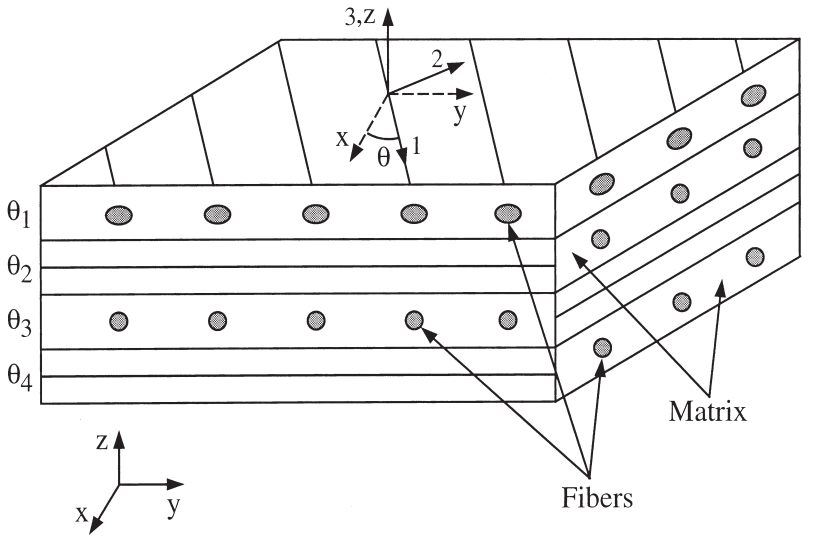

Fig. 2. Material and element coordinate systems for a fiber-composite laminate.

$$\{\tau'\}=[Q_2']\{\gamma'\} \tag{7}$$

where

$$[Q_1']=\begin{bmatrix} \dfrac{E_{11}}{1-\nu_{12}\nu_{21}} & \dfrac{\nu_{12}E_{22}}{1-\nu_{12}\nu_{21}} & 0 \\ \dfrac{\nu_{21}E_{11}}{1-\nu_{12}\nu_{21}} & \dfrac{E_{22}}{1-\nu_{12}\nu_{21}} & 0 \\ 0 & 0 & G_{12} \end{bmatrix} \tag{8}$$

$$[Q_2']=\begin{bmatrix} \alpha_1 G_{13} & 0 \\ 0 & \alpha_2 G_{23} \end{bmatrix} \tag{9}$$

where $\{\sigma'\}=\{\sigma_1, \sigma_2, \tau_{12}\}^T$, $\{\tau'\}=\{\tau_{13}, \tau_{23}\}^T$, $\{\varepsilon'\}=\{\varepsilon_1, \varepsilon_2, \gamma_{12}\}^T$, $\{\gamma'\}=\{\gamma_{13}, \gamma_{23}\}^T$. The α_1 and α_2 are shear correction factors. In ABAQUS, the shear correction factors are calculated by assuming that the transverse shear energy through the thickness of laminate is equal to that of the case of unidirectional bending [13,17].

Let $\{\sigma\}=\{\sigma_x, \sigma_y, \tau_{xy}\}^T$, $\{\tau\}=\{\tau_{xz}, \tau_{yz}\}^T$, $\{\varepsilon\}=\{\varepsilon_x, \varepsilon_y, \gamma_{xy}\}^T$, $\{\gamma\}=\{\gamma_{xz}, \gamma_{yz}\}^T$. Then constitutive equations for the lamina in the element coordinates (x,y,z) then become

$$\{\sigma\}=[Q_1]\{\varepsilon\}, \tag{10}$$

$$\{\tau\}=[Q_2]\{\gamma\}, \tag{11}$$

and

$$[Q_1]=[T_1]^T[Q_1'][T_1] \tag{12}$$

$$[Q_2]=[T_2]^T[Q_2']\,[T_2] \tag{13}$$

$$[T_1]=\begin{bmatrix}\cos^2\theta & \sin^2\theta & \sin\theta\cos\theta\\ \sin^2\theta & \cos^2\theta & -\sin\theta\cos\theta\\ -2\sin\theta\cos\theta & 2\sin\theta\cos\theta & \cos^2\theta-\sin^2\theta\end{bmatrix} \tag{14}$$

$$[T_2]=\begin{bmatrix}\cos\theta & \sin\theta\\ -\sin\theta & \cos\theta\end{bmatrix} \tag{15}$$

where the fiber orientation θ is measured counterclockwise from the element local x-axis to the material 1-axis.

Let $\{\varepsilon_0\}=\{\varepsilon_{x0},\varepsilon_{y0},\gamma_{xy0}\}^T$ be the in-plane strains at the mid-surface of the laminate section, $\{\kappa\}=\{\kappa_x,\ \kappa_y,\ \kappa_{xy}\}^T$ the curvatures, and h the total thickness of the section. If there are n layers in the layup, the stress resultants, $\{N\}=\{N_x,\ N_y,\ N_{xy}\}^T$, $\{M\}=\{M_x,\ M_y,\ M_{xy}\}^T$ and $\{V\}=\{V_x,\ V_y\}^T$, can be defined as

$$\begin{Bmatrix}\{N\}\\ \{M\}\\ \{V\}\end{Bmatrix}=\int_{-h/2}^{h/2}\begin{Bmatrix}\{\sigma\}\\ z\{\sigma\}\\ \{\tau\}\end{Bmatrix}dz=\int_{-h/2}^{h/2}\begin{Bmatrix}[Q_1]\{\varepsilon\}\\ z[Q_1]\{\varepsilon\}\\ [Q_2]\{\gamma\}\end{Bmatrix}dz=\int_{-h/2}^{h/2}\begin{Bmatrix}[Q_1](\{\varepsilon_0\}+z\{\kappa\})\\ z[Q_1](\{\varepsilon_0\}+z\{\kappa\})\\ [Q_2]\{\gamma\}\end{Bmatrix}dz \tag{16}$$

or

$$\begin{Bmatrix}\{N\}\\ \{M\}\\ \{V\}\end{Bmatrix}=\sum_{j=1}^{n}\begin{bmatrix}(z_{jt}-z_{jb})[Q_1] & \frac{1}{2}(z_{jt}^2-z_{jb}^2)[Q_1] & [0]\\ \frac{1}{2}(z_{jt}^2-z_{jb}^2)[Q_1] & \frac{1}{3}(z_{jt}^3-z_{jb}^3)[Q_1] & [0]\\ [0]^T & [0]^T & (z_{jt}-z_{jb})[Q_2]\end{bmatrix}\begin{Bmatrix}\{\varepsilon_0\}\\ \{\kappa\}\\ \{\gamma\}\end{Bmatrix} \tag{17}$$

where z_{jt} and z_{jb} are the distance from the mid-surface of the section to the top and the bottom of the jth layer, respectively. The [0] is a 3 by 2 matrix with all the coefficients equal to zero.

Prior to numerical analyses, the ABAQUS program has been employed to analyze the buckling of composite cylindrical panels with cutout and buckling of isotropic skew plates. These solutions are compared with known benchmark solutions [11] and satisfactory results are obtained [18].

4. Results of the numerical analysis

4.1. Laminate rhombus plates

In this section composite laminate rhombus plates subjected to uniaxial compressive force N per unit length as shown in Fig. 1 are analyzed. The plates do not have any circular cutouts (d=0). The length and width of the plates are a=b=10 cm and the skew angle α varies between 50° and 90°. Two types of edge conditions are considered, which are four edges simply supported (Fig. 1(a)) and four edges clamped (Fig. 1(b)). These end conditions prevent out of plane displacement w but allow in-plane movements u and v. The lamina in the plates consists of graphite/epoxy (Hercules AS/3501-6) and material constitutive properties are taken from Crawley [19], which are E_{11}=128 GPa, E_{22}=11 GPa, ν_{12}=0.25, G_{12}=G_{13}=4.48 GPa, G_{23}=1.53 GPa. The thickness of each ply is 0.125 mm. Eight types of laminate layups, $[90/0]_{2s}$, $[\alpha/0]_{2s}$, $[90/45/0/-45]_{s}$, $[\pm\theta]_{2s}$, $[90/0]_{10s}$, $[\alpha/0]_{10s}$, $[90/45/0/-45]_{5s}$, and $[\pm\theta]_{10s}$ are studied. In the finite element analysis, no symmetry simplifications are made and a 10×10 finite element mesh (100 elements) is used to model the entire rhombus plate.

Fig. 3 shows critical buckling load N_{cr} versus the skew angle α for $[90/0]_{2s}$, $[\alpha/0]_{2s}$, $[90/45/0/-45]_{s}$ composite rhombus plates. We can see that the critical buckling loads of the plates generally decrease with the increase of angle α. Under the simply supported conditions, the $[\alpha/0]_{2s}$ plates, with fibers parallel to edges, always have the lowest buckling loads and the quasi-isotropic $[90/45/0/-45]_{s}$ plates usually have the highest buckling loads (except $\alpha<60°$). When the edges of plates are all clamped, the results of analyses are quite different. The $[90/0]_{2s}$, plates have the highest buckling loads and the $[90/45/0/-45]_{s}$ plates have the lowest buckling loads.

Fig. 4 shows critical buckling load N_{cr} versus the skew angle α for $[90/0]_{10s}$, $[\alpha/0]_{10s}$, $[90/45/0/-45]_{5s}$, composite rhombus plates. For plates with simply supported conditions, except for the magnitude of the buckling loads, the results of analysis for these thicker plates (Fig. 4(a)) are very similar to those of thin plates (Fig. 3(a)). Comparing Fig. 4(b) with Fig. 3(b), we can observe that the thickness does have some influence on the buckling behavior of clamped rhombus plates. First, the buckling loads of the $[\alpha/0]_{10s}$ plates may increase with the skew angle α when $\alpha>60°$. Second, the buckling loads of $[90/45/0/-45]_{5s}$ plates may be greater than those of $[\alpha/0]_{10s}$ plates when $\alpha<70°$.

Fig. 5 shows the typical buckling modes of $[90/0]_{2s}$, $[\alpha/0]_{2s}$, $[90/45/0/-45]_{s}$ composite rhombus plates with different edge conditions for plate skew angle α equal to 50° and 90°. From the figure we can observe that when the skew angle is small, the buckling modes of the plate tend to have more waves in the inplane loading direction. In addition, the buckling modes of the plates with clamped edges tend to have more wave than those with simply supported edges. The buckling modes of $[90/0]_{10s}$, $[\alpha/0]_{10s}$, $[90/45/0/-45]_{5s}$, plates show the similar trend as the thin plates [18] and are not plotted here.

The last rhombus plates for analysis are the angle ply $[\pm\theta]_{2s}$ and $[\pm\theta]_{10s}$ laminate plates, in which $0°\leq\theta\leq90°$. Fig. 6(a) shows that if the angle θ is fixed, the critical

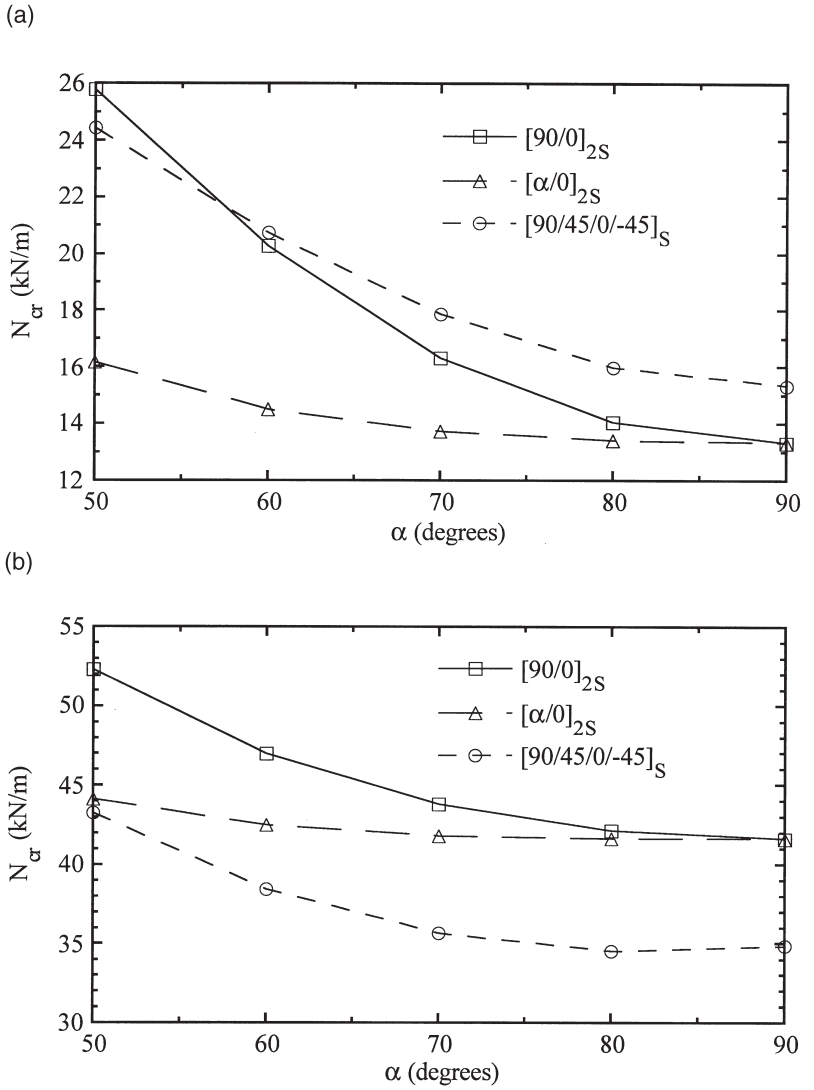

Fig. 3. Effect of skew angle on buckling loads of composite rhombus plates with $[90/0]_{2s}$, $[\alpha/0]_{2s}$, and $[90/45/0/-45]_s$ laminate layups: (a) simply supported edges; (b) clamped edges.

buckling loads of simply supported $[\pm\theta]_{2s}$ plates increase with the decrease of the skew angle α. When the angle α is smaller, this increase in buckling loads is more prominent. In addition, when the skew angle α is large, the highest buckling loads of the composite plates seem to take place with fiber angle θ close to 45°. However, when the skew angle α is small, the highest buckling load may occur with θ shifting to high values (say 55°). From Fig. 6(b) we can see that when the plate thickness

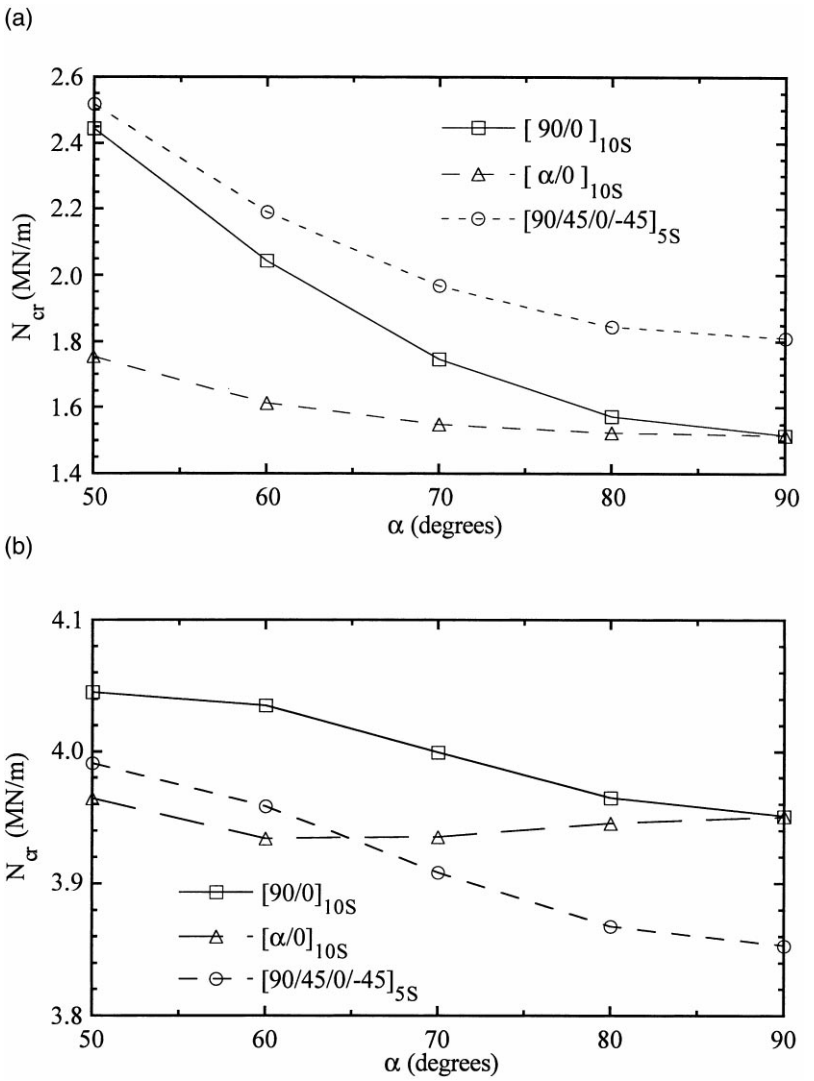

Fig. 4. Effect of skew angle on buckling loads of composite rhombus plates with $[90/0]_{10s}$, $[\alpha/0]_{10s}$, and $[90/45/0/-45]_{10s}$ laminate layups: (a) simply supported edges; (b) clamped edges.

is increased, the highest buckling loads of the simply supported $[\pm\theta]_{10s}$ plates all seem to occur with θ around 45°.

If the edge conditions of these plates are changed to clamped edges, we can observe from Fig. 7(a) that the critical buckling loads of the plates still increase with the decrease of the skew angle α. It seems that the highest buckling loads of most of the plates take place with the fiber angle θ close to 0°. The only two exceptions are the plates with α equal to 50° and 60°, where the highest buckling loads take

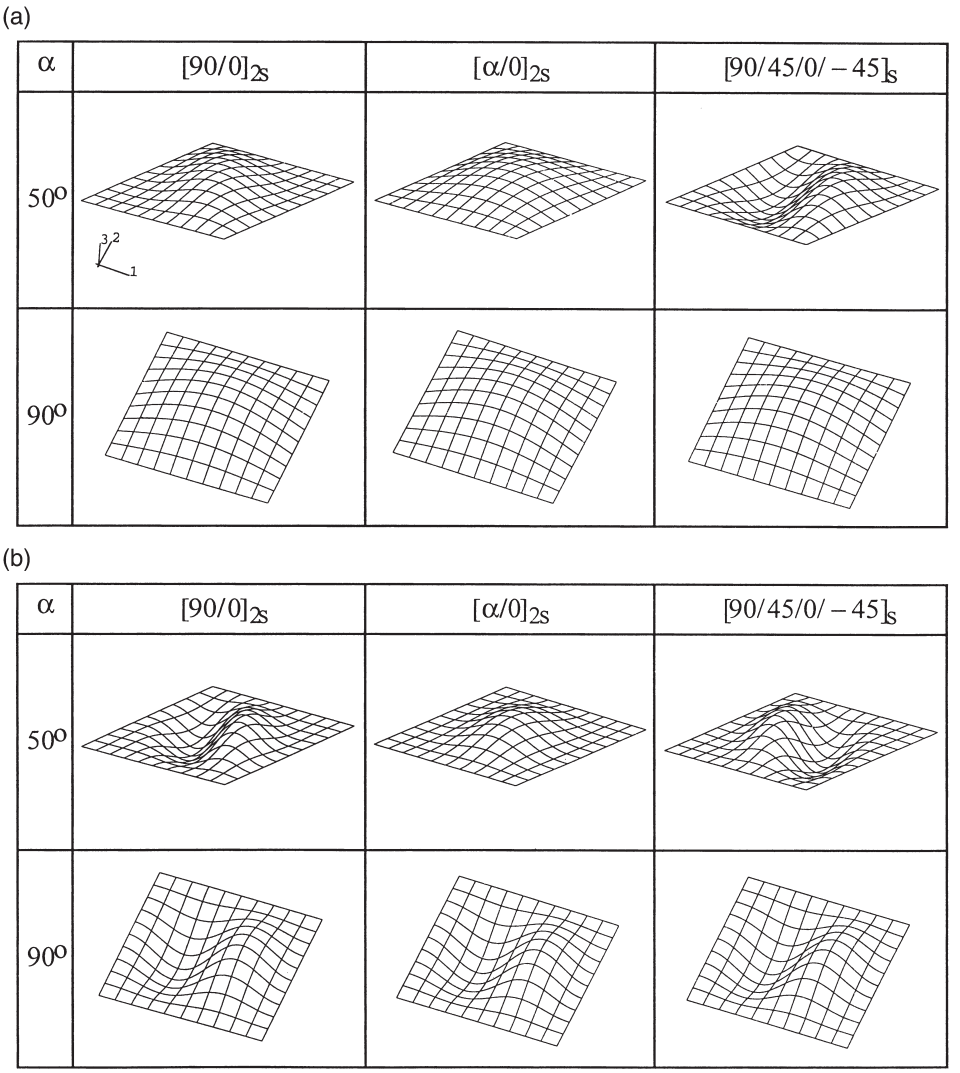

Fig. 5. Buckling modes of composite rhombus plates with $[90/0]_{2s}$, $[\alpha/0]_{2s}$, and $[90/45/0/-45]_s$ laminate layups: (a) plates with simply supported edges; (b) plates with clamped edges.

place with θ around 40°. If the plate thickness is increased, the highest buckling loads of the clamped $[\pm\theta]_{10s}$ plates almost all take place with θ close to 0° as shown in Fig. 7(b). The only exception is the plate with α equal to 50°, where the highest buckling load occurs with θ around 20°.

Comparing Fig. 6 with Fig. 7, we can observe that the edge conditions have significant influence on the buckling behavior of the rhombus plates. In addition, when the plate thickness is increased, the highest buckling load of rhombus plates with angle ply laminate layup will more consistently take place at the same θ angle (say,

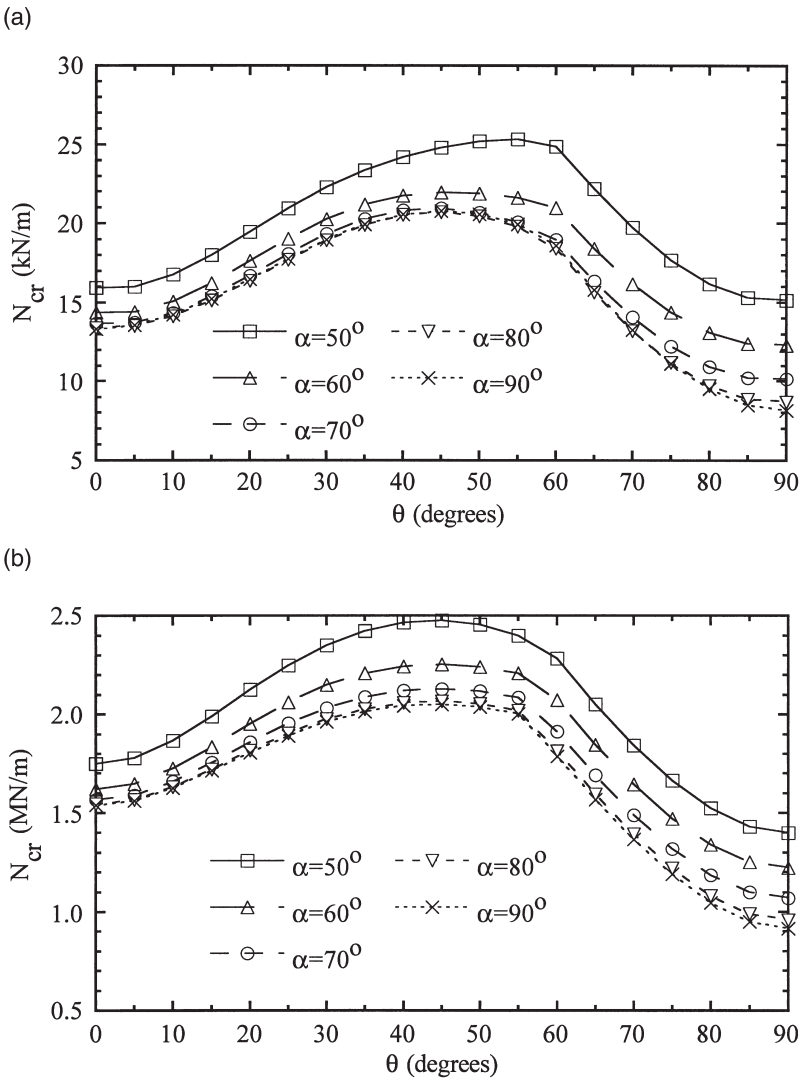

Fig. 6. Effect of skew angle on buckling loads of simply supported $[\pm\theta]_{2s}$, and $[\pm\theta]_{10s}$ composite rhombus plates: (a) $[\pm\theta]_{2s}$ plate; (b) $[\pm\theta]_{10s}$ plate.

θ=45° for simply supported plates and θ=0° for clamped plates). Hence, it may be suggested to use θ=45° in the design of simply supported rhombus plates with angle ply $[\pm\theta]_{ns}$ laminate layup and subjected to uniaxial compressive loading. Though, in some cases, there would have been other better θ angles to achieve higher buckling resistance of plates. However, as far as simplicity is concerned, the use of the $[\pm 45]_{ns}$ laminate layup may be a straightforward and practical choice. On the same basis, it may also be suggested to use the $[0_2]_{ns}$ laminate layup (all fibers parallel to the

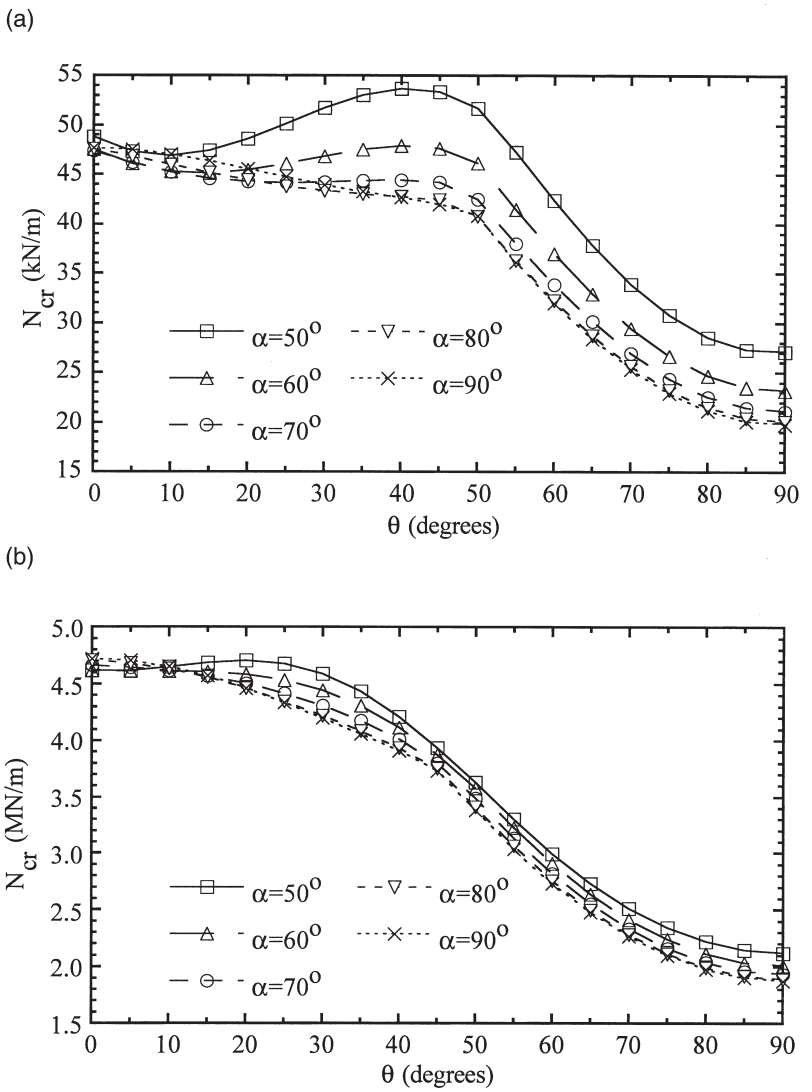

Fig. 7. Effect of skew angle on buckling loads of clamped $[\pm\theta]_{2s}$ and $[\pm\theta]_{10s}$ composite rhombus plates: (a) $[\pm\theta]_{2s}$ plate; (b) $[\pm\theta]_{10s}$ plate.

loading direction) in the design of clamped rhombus plates subjected to uniaxial compression.

Fig. 8 shows the typical buckling modes of $[\pm 0]_{2s}$, $[\pm 45]_{2s}$, and $[\pm 90]_{2s}$ composite rhombus plates with different edge conditions for plate skew angle α equal to 50° and 90°. It shows that the buckling modes of the $[\pm 90]_{2s}$ plate usually have more waves than those of $[\pm 0]_{2s}$ and $[\pm 45]_{2s}$, plates. Again, the buckling modes of the plate with clamped edges tend to have more waves than those with simply supported

(a)

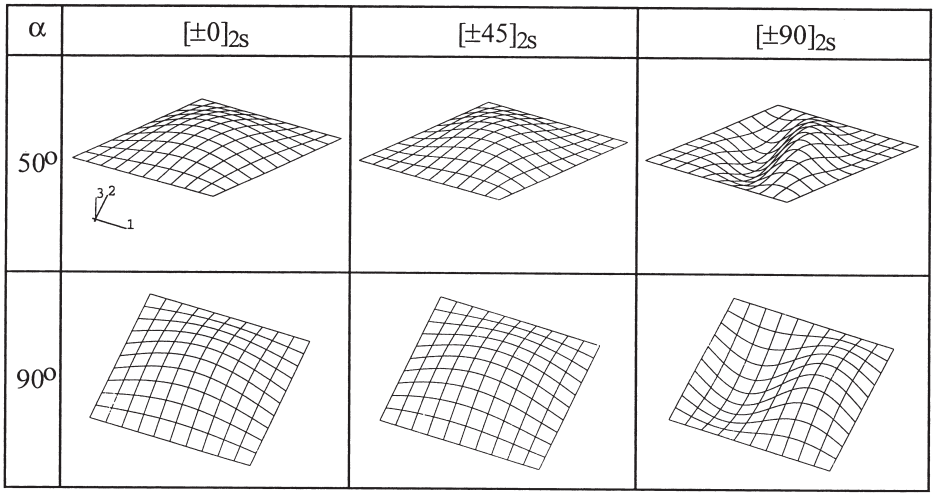

(b)

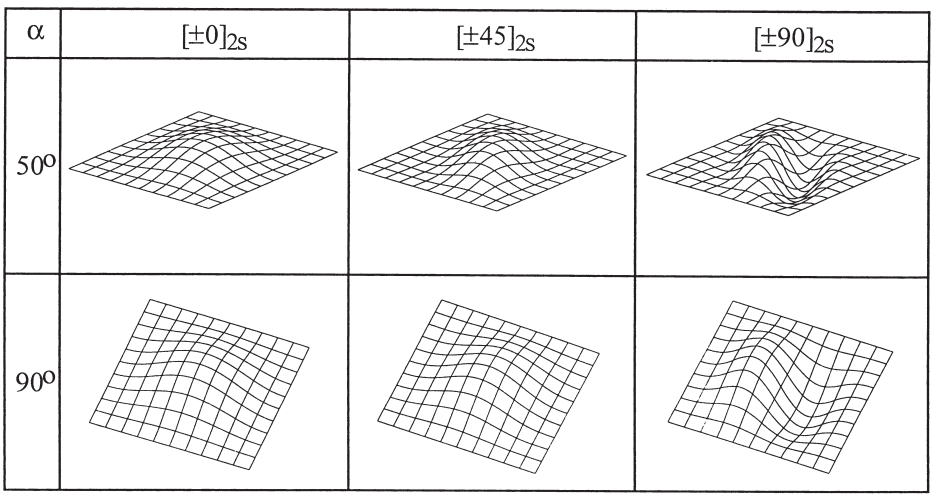

Fig. 8. Buckling modes of composite rhombus plates with $[\pm 0]_{2s}$, $[\pm 45]_{2s}$, and $[\pm 90]_{2s}$ laminate layups: (a) plates with simply supported edges; (b) plates with clamped edges.

edges. The buckling modes of $[\pm 0]_{10s}$, $[\pm 45]_{10s}$, and $[\pm 90]_{10s}$ plates show a similar trend as the thin plates [18] and are not plotted here.

4.2. Laminate parallelogram plates with various aspect ratios

In this section composite laminate parallelogram plates subjected to uniaxial loading are analyzed (Fig. 1). The plates do not have any circular cutouts (d=0). The laminate layups are $[\pm\theta]_{ns}$, in which n=2, 10, and $0° \leq \theta \leq 90°$. The width b of the

plates is 10 cm. The length a of the plates may be either 5 cm (a/b=0.5) or 40 cm (a/b=4). The skew angle α of the plates still varies between 50° and 90° and two types of boundary conditions, four edges simply supported and four edges clamped, are considered. Again, no symmetry simplifications are made in the analysis. A 10×10 finite element mesh (100 elements) is used to model the plates with a/b=0.5 and a 10×20 finite element mesh (200 elements) is used to model the plates with a/b=4.

Fig. 9 shows critical buckling load N_{cr} versus the angle θ for $[\pm\theta]_{2s}$ and $[\pm\theta]_{10s}$ composite parallelogram plates with a/b=0.5 and with four simply supported edges. We can see that the maximum buckling loads of the $[\pm\theta]_{2s}$ thin plates all take place when the θ angle is equal to 0° (Fig. 9(a)). For thick plates with $[\pm\theta]_{10s}$ laminate layup (Fig. 9(b)), the maximum buckling loads also take place at θ equal to 0° for most cases. The only exception is the plate with skew angle α equal to 50°, where the maximum buckling load may occur with θ around 25°. We can observe that for both thin and thick plates with large θ angle, the critical buckling loads generally decrease with the increase of angle α. However, when the θ angle is close to 0°, this trend is totally reversed and the critical buckling loads decrease with the decrease of angle α.

Fig. 10 shows critical buckling load N_{cr} versus the angle θ for $[\pm\theta]_{2s}$ and $[\pm\theta]_{10s}$ composite parallelogram plates with a/b=0.5 and with four clamped edges. For $[\pm\theta]_{2s}$, thin plates (Fig. 10(a)), the trends of the buckling behavior are similar to those of plates with simply supported edges except the buckling loads are increased. For $[\pm\theta]_{10s}$ thick plates (Fig. 10(b)), it can be seen that when the θ angle is greater than 25°, the critical buckling loads increase with the decrease of angle α. When the θ angle is less than 25°, the critical buckling loads increase with the increase of angle α.

Fig. 11 shows critical buckling load N_{cr} versus the angle θ for $[\pm\theta]_{2s}$ and $[\pm\theta]_{10s}$ composite parallelogram plates with a/b=4 and with four simply supported edges. We can see that the maximum buckling loads of the $[\pm\theta]_{10s}$, plates take place with the θ angle around 45° and that the maximum buckling loads of the $[\pm\theta]_{10s}$ plates take place with the θ angle around 40°. For both thin and thick plates, the critical buckling loads all decrease with the increase of the α angle. When the edge condition of the long plates is changed to clamped, we can observe from Fig. 12(a) that the edge conditions do not have significant influence on the trends of the buckling behavior of the $[\pm\theta]_{2s}$, thin plates (except the buckling loads are increased). Comparing Fig. 12(b) with Fig. 11(b), we can observe that the clamped edge conditions shift the optimal fiber angle θ from around 40° to around 35°. Finally, comparing Figs. 11 and 12 with Figs. 9 and 10, we can see that the optimal fiber angle θ for $[\pm\theta]_{2s}$ and $[\pm\theta]_{10s}$ skew plates is influenced by the plate aspect ratio significantly. When the plate is short, the optimal angle θ is usually close to 0°. However, when the plate is long, the optimal angle θ is usually between 35° and 45°.

Fig. 13 shows the typical buckling modes of $[\pm0]_{2s}$, $[\pm45]_{2s}$ and $[\pm90]_{2s}$ clamped composite parallelogram plates with aspect ratio a/b equal to 0.5 and 4 and plate skew angle α equal to 50° and 90°. It shows that the buckling modes of plates with large aspect ratio and small skew angle usually have more waves than those of plates

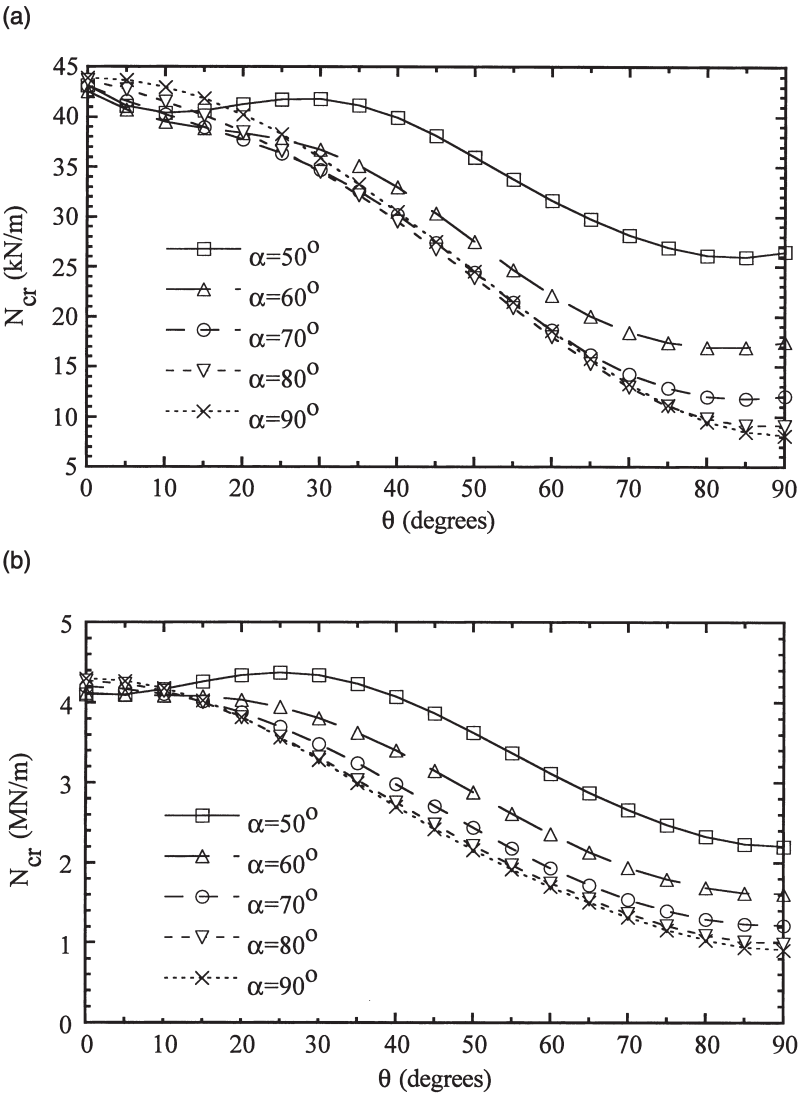

Fig. 9. Effect of skew angle on buckling loads of simply supported $[\pm\theta]_{2s}$ and $[\pm\theta]_{10s}$ composite parallelogram plates with a/b=0.5: (a) $[\pm\theta]_{2s}$ plate; (b) $[\pm\theta]_{10s}$ plate.

with small aspect ratio and large skew angle. In addition, for plates with large aspect ratio, the buckling modes of the $[\pm 90]_{2s}$ plate usually have more waves than those of $[\pm 0]_{2s}$ and $[\pm 45]_{2s}$ plates. The buckling modes of thin plates with simply supported edges as well as thick plates with simply supported edges or clamped edges show a similar trend [18].

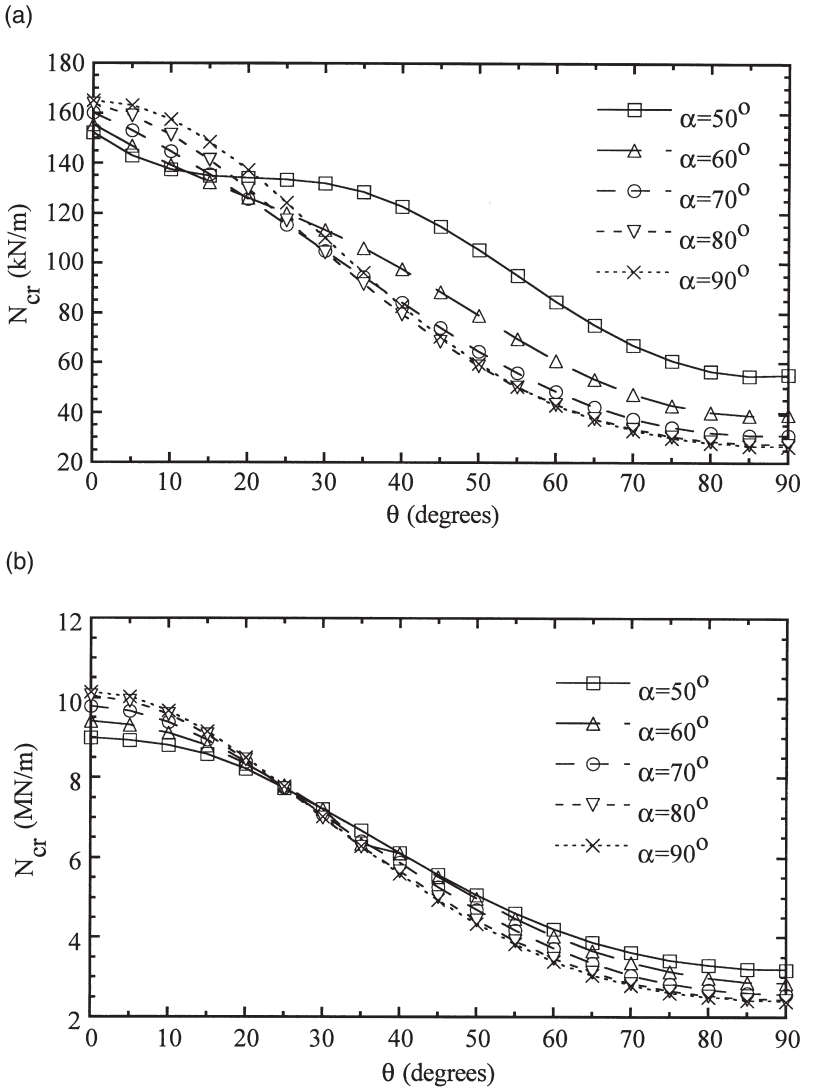

Fig. 10. Effect of skew angle on buckling loads of clamped $[\pm\theta]_{2s}$ and $[\pm\theta]_{10s}$ composite parallelogram plates with a/b=0.5: (a) $[\pm\theta]_{2s}$ plate; (b) $[\pm\theta]_{10s}$ plate.

4.3. Laminate parallelogram plates with various aspect ratios and circular cutouts

In this section laminate parallelogram plates with central circular cutouts and subjected to uniaxial loading are analyzed (Fig. 1). The laminate layup is $[\pm\theta]_{2s}$, and $0°\leq\theta\leq90°$. The width b of the plates is 10 cm. The length a of the plates may be either 5 cm (a/b=0.5) or 40 cm (a/b=4). In the analysis, the diameter d of the cutout

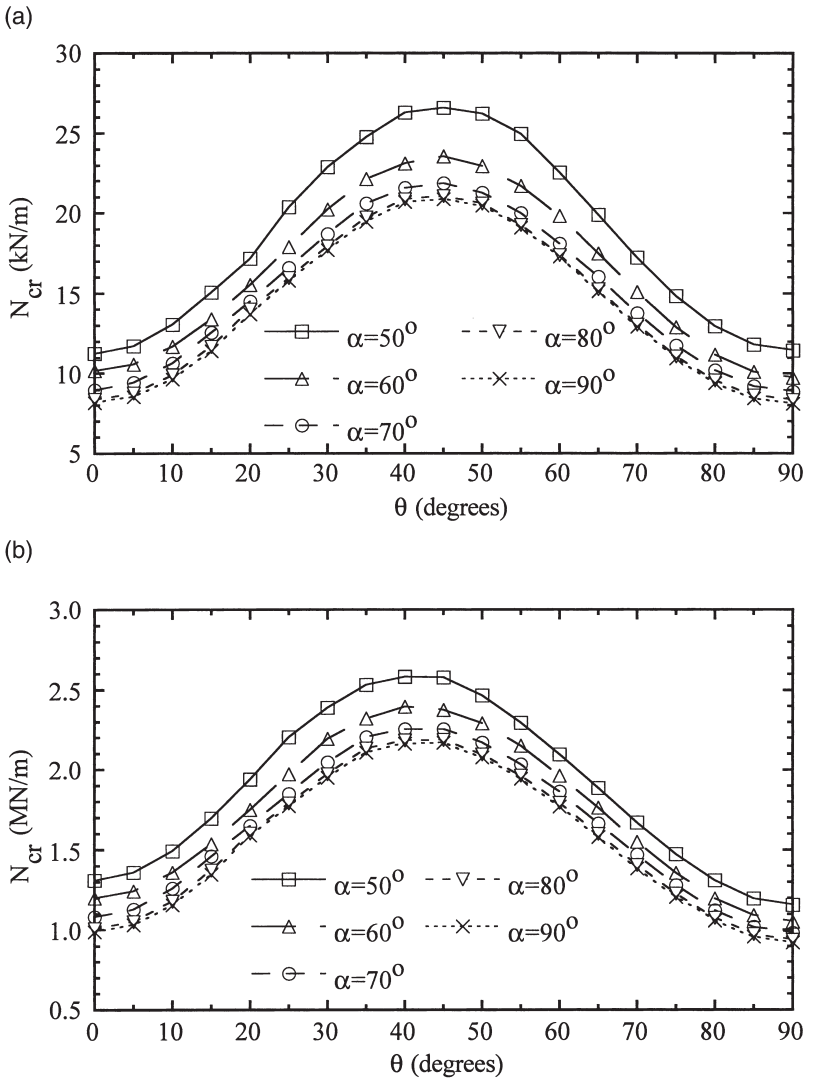

Fig. 11. Effect of skew angle on buckling loads of simply supported $[\pm\theta]_{2s}$ and $[\pm\theta]_{10s}$ composite parallelogram plates with a/b=4: (a) $[\pm\theta]_{2s}$ plate; (b) $[\pm\theta]_{10s}$ plate.

is 2 cm (d/b=0.2). The skew angle α of the plates still varies between 50° and 90° and two types of boundary conditions, four edges simply supported and four edges clamped, are considered. No symmetry simplifications are made in the analysis. Due to the presence of cutouts, at least 500 elements are used to model the plates with a/b=0.5 and at least 800 elements are used to model the plates with a/b=4.

Fig. 14 shows critical buckling load N_{cr} versus the angle θ for $[\pm\theta]_{2s}$ composite parallelogram plates with a/b=0.5 and with cutout. Comparing Fig. 14(a) with Fig.

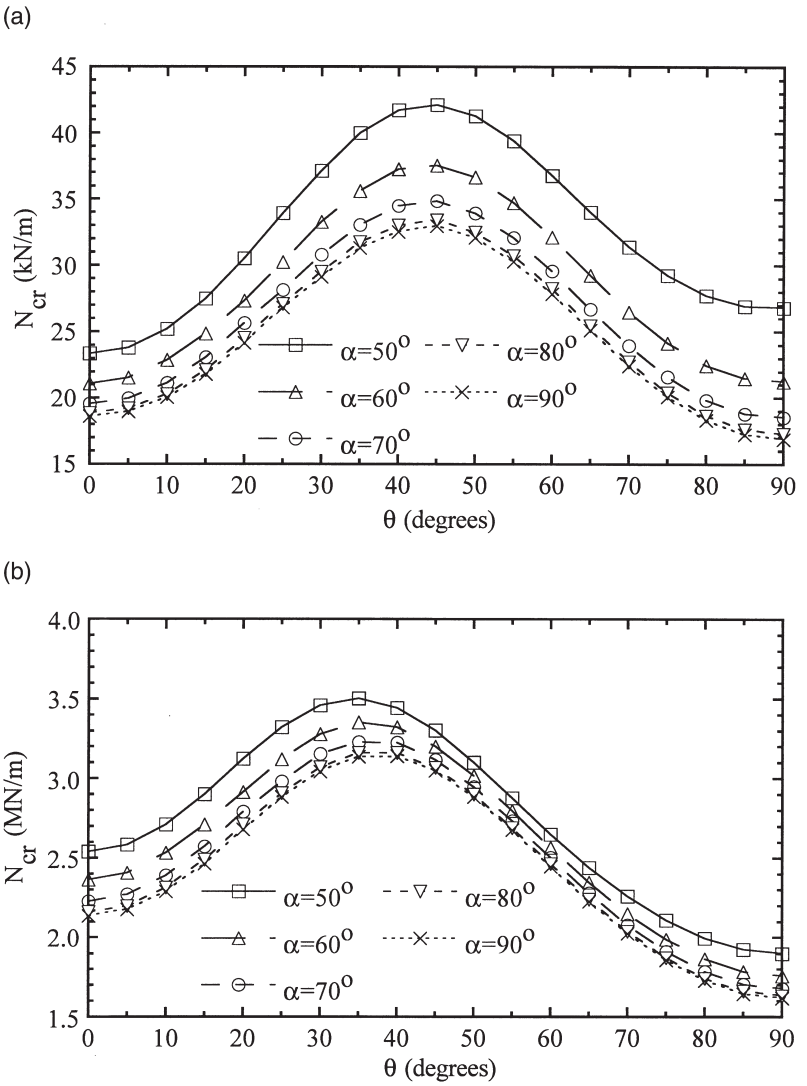

Fig. 12. Effect of skew angle on buckling loads of clamped $[\pm\theta]_{2s}$ and $[\pm\theta]_{10s}$ composite parallelogram plates with a/b=4: (a) $[\pm\theta]_{2s}$ plate; (b) $[\pm\theta]_{10s}$ plate.

9(a), and comparing Fig. 14(b) with Fig. 10(a), we can see that no matter what the edge conditions, the N_{cr} verses θ curves of short skew plates with central holes are very similar to those of plates without holes. The only difference is that the critical buckling loads of plates with holes are lower than those of plates without cutouts. Fig. 15(a) shows the reductions (in percentage) of the critical buckling loads for simply supported plates with a/b=0.5 and with cutout. It seems that under the same fiber angle θ, the plates having small α angles usually have large reductions in the

(a)

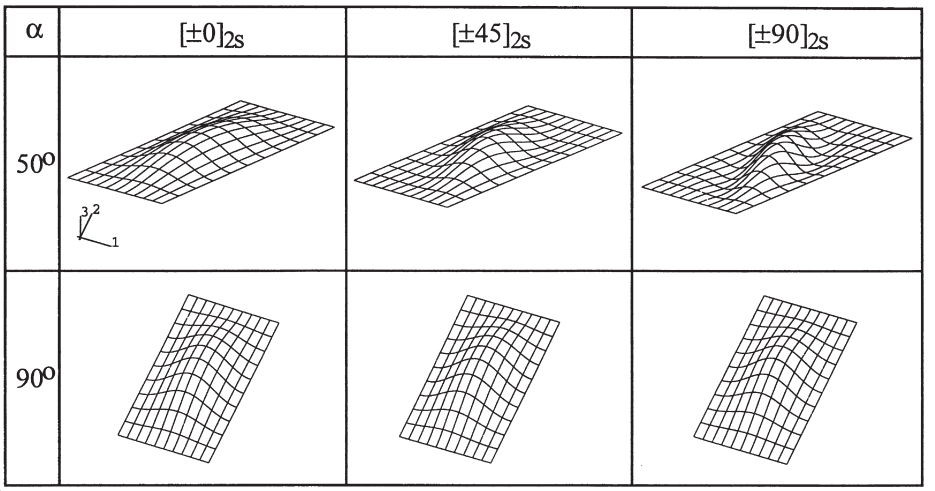

(b)

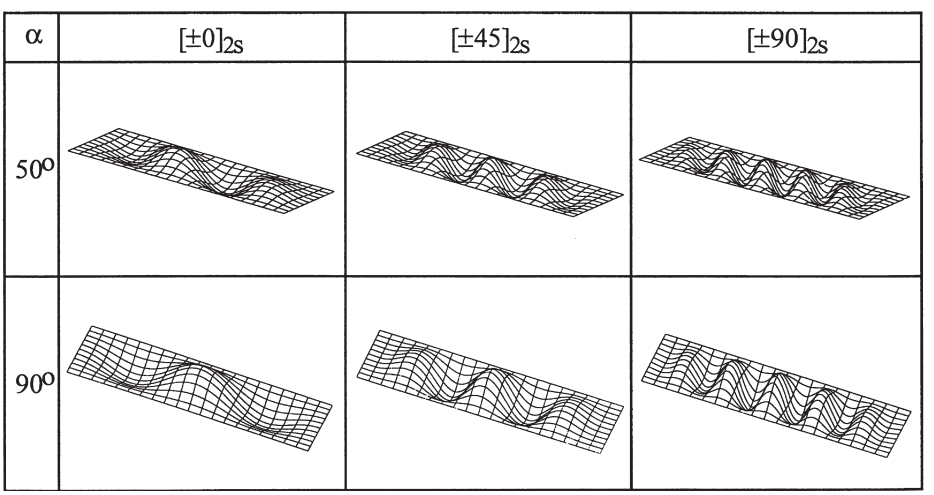

Fig. 13. Buckling modes of clamped composite parallelogram plates with $[\pm 0]_{2s}$, $[\pm 45]_{2s}$, and $[\pm 90]_{2s}$ laminate layups: (a) $a/b = 0.5$; (b) $a/b = 4$.

critical buckling loads. However, this trend is totally reversed for small θ angle. When the θ angle is less than 15°, the plates having large α angles will have large reductions in the critical buckling loads. Fig. 15(b) shows the reduction of the critical buckling loads for clamped plates with a/b=0.5 and with cutout. The curves show similar trends as the plate with simply supported edges. However, the reduction rates in critical buckling loads of plates with clamped edges are usually smaller than those of plates with simply supported edges.

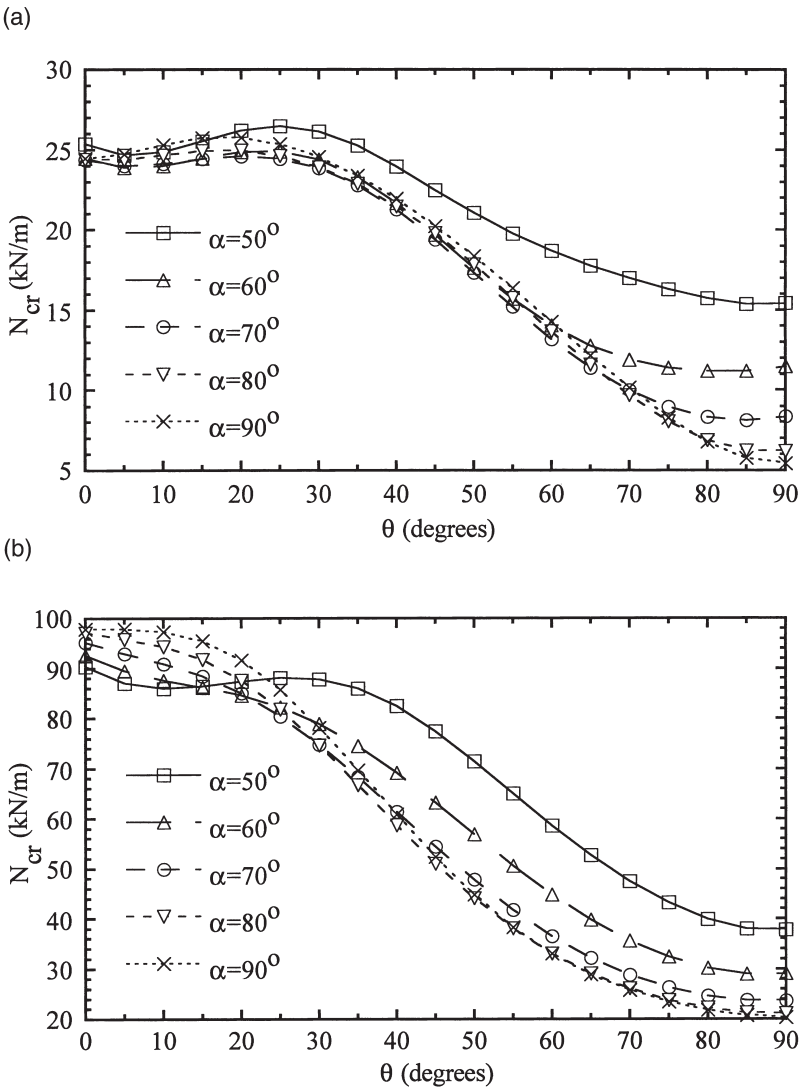

Fig. 14. Effect of skew angle on buckling loads of $[\pm\theta]_{2S}$ composite parallelogram plates with a central circular cutout (a/b=0.5 and d/b=0.2): (a) simply supported edges; (b) clamped edges.

Fig. 16 shows critical buckling load N_{cr} versus the angle θ for $[\pm\theta]_{2s}$ composite parallelogram plates with a/b=4 and with cutout. Comparing Fig. 16(a) with Fig. 11(a), and comparing Fig. 16(b) with Fig. 12(a), we can observe that the curves of long skew plates with central holes are again very similar to those of plates without holes. Fig. 17 shows the reductions of the critical buckling loads for plates with a/b=4 and with cutout. Again, it seems that for large θ angle, the plates having small skew angle α usually have large reductions in the critical buckling loads. For small

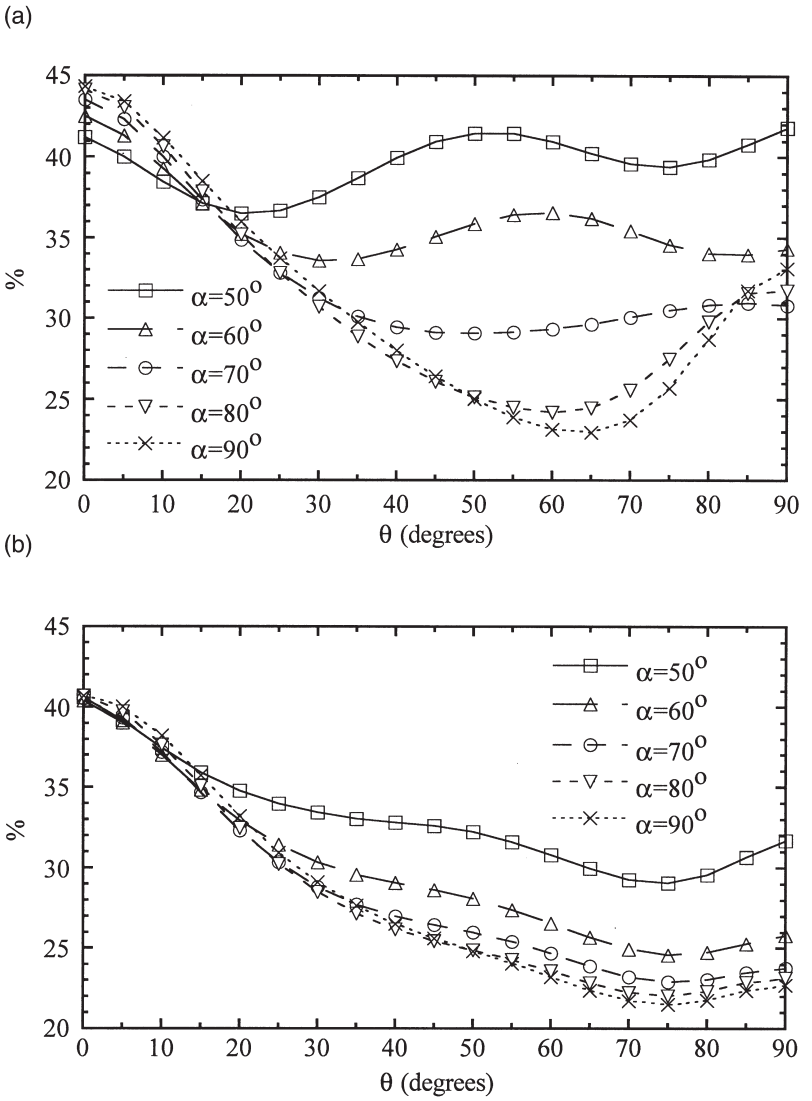

Fig. 15. Reduction of critical buckling load for $[\pm\theta]_{2S}$ composite parallelogram plates with a central circular cutout (a/b=0.5 and d/b=0.2: (a) simply supported edges; (b) clamped edges.

θ angle, the plates having large skew angle α usually have large reductions in the critical buckling loads. It should be noted that there are some negative values of reductions in buckling loads for plates with small θ angle and large α angle. This means that the plates with cutouts may have higher critical buckling loads than the same plates without holes, which is quite different from our intuition. However, past research did show (numerically and experimentally) that introducing a hole into an isotropic plate or a composite plate does not always reduce the buckling load and,

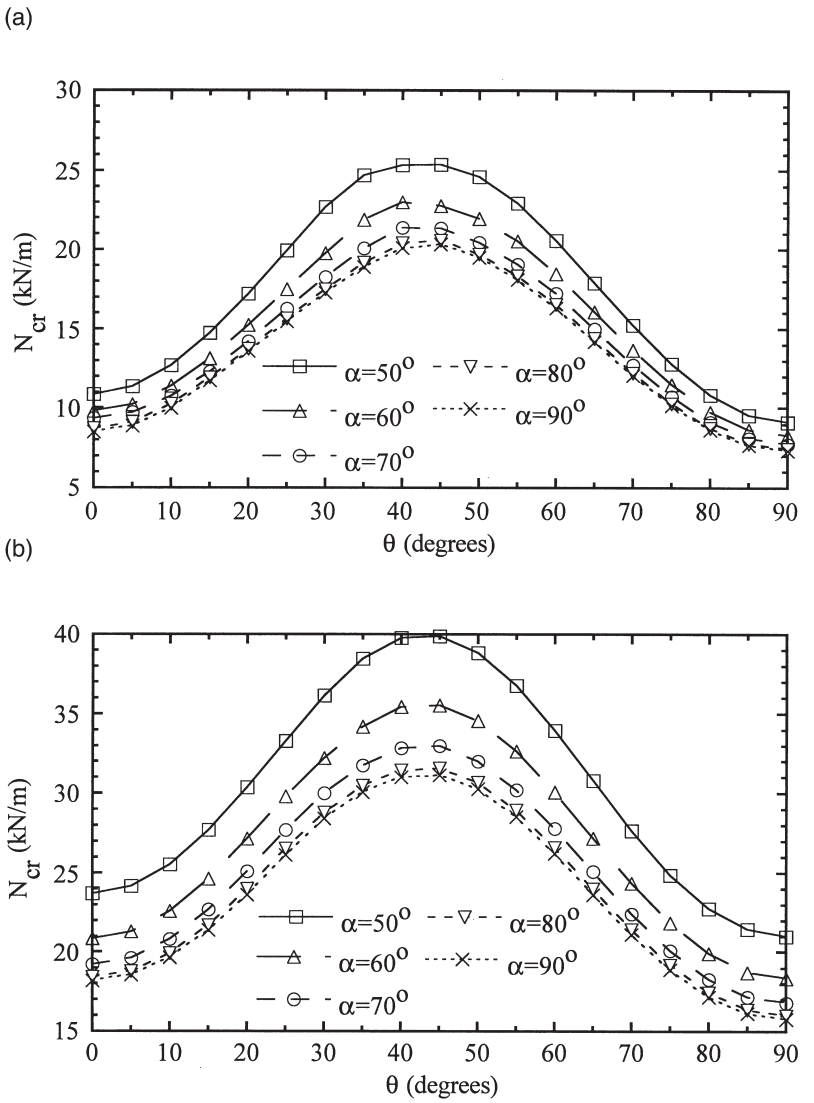

Fig. 16. Effect of skew angle on buckling loads of $[\pm\theta]_{2S}$ composite parallelogram plates with a central circular cutout (a/b=4 and d/b=0.2): (a) simply supported edges; (b) clamped edges.

in some instances, may increase its buckling load [6,7,20]. This is because the buckling load of a plate is not only influenced by a cutout, but is also influenced by material orthotropy, end condition, and plate geometry. Comparing Fig. 17 with Fig. 15, we can observe that the changes of critical buckling loads due to the presence of cutouts for short skew plates are more significant than those for long skew plates.

Finally, Fig. 18 shows the typical buckling modes of $[\pm0]_{2s}$, $[\pm45]_{2s}$ and $[\pm90]_{2s}$ clamped composite parallelogram plates with central cutout, with aspect ratio a/b

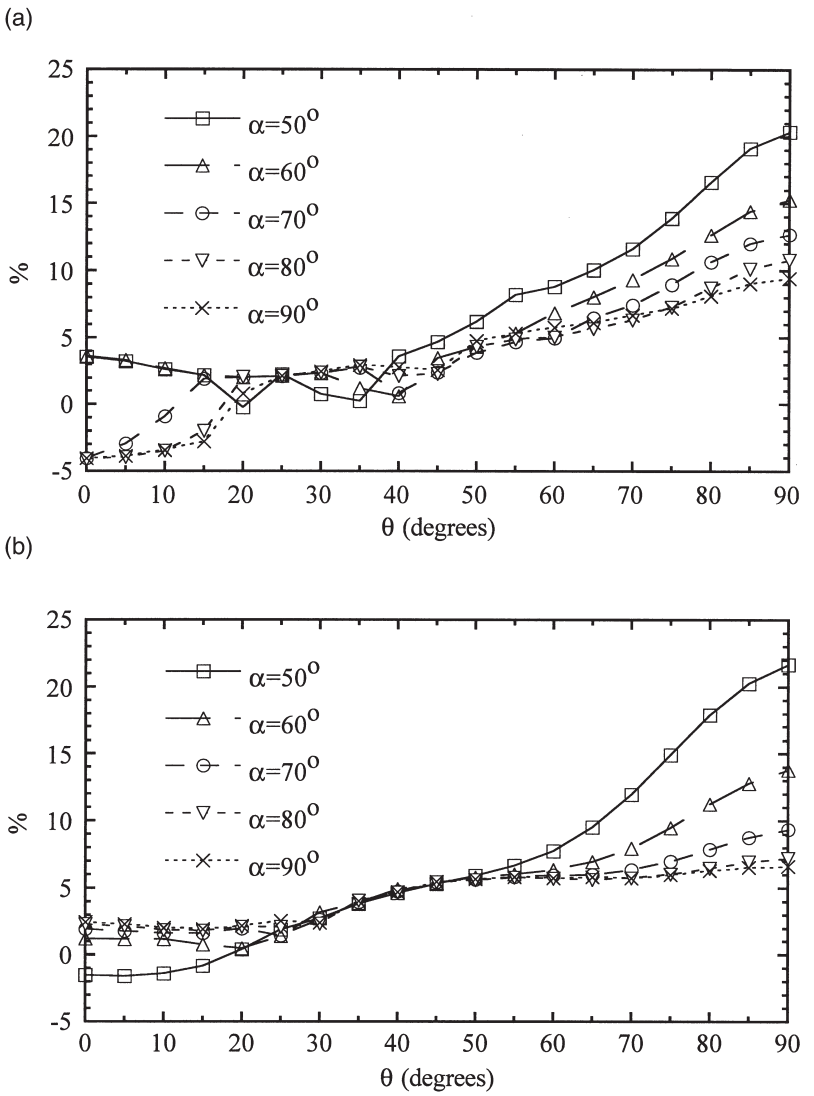

Fig. 17. Reduction of critical buckling load for $[\pm\theta]_{2S}$ composite parallelogram plates with a central circular cutout (a/b=4 and d/b=0.2): (a) simply supported edges; (b) clamped edges.

equal to 0.5 and 4 and with plate skew angle α equal to 50° and 90°. Comparing Fig. 18 with Fig. 13, we can observe that the introduction of cutouts may cause the buckling modes of long plates to have fewer numbers of waves in the loading direction than those of plates without cutouts.

(a)

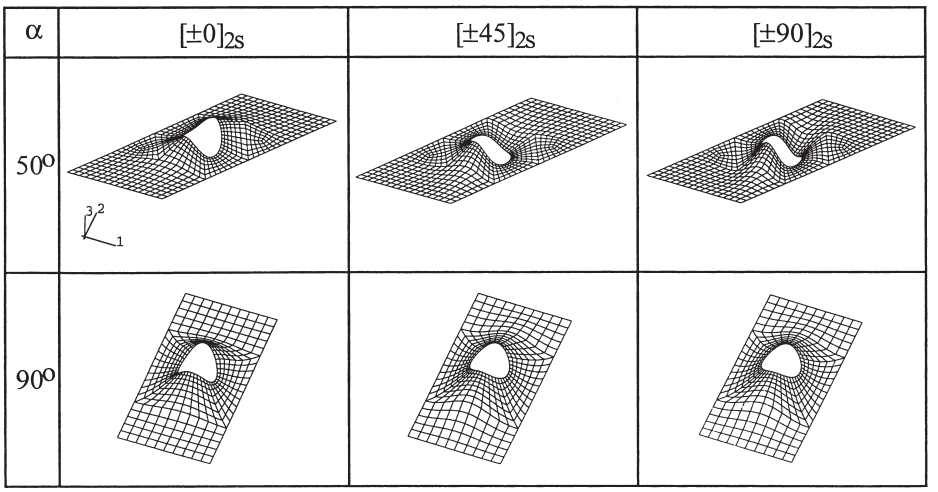

(b)

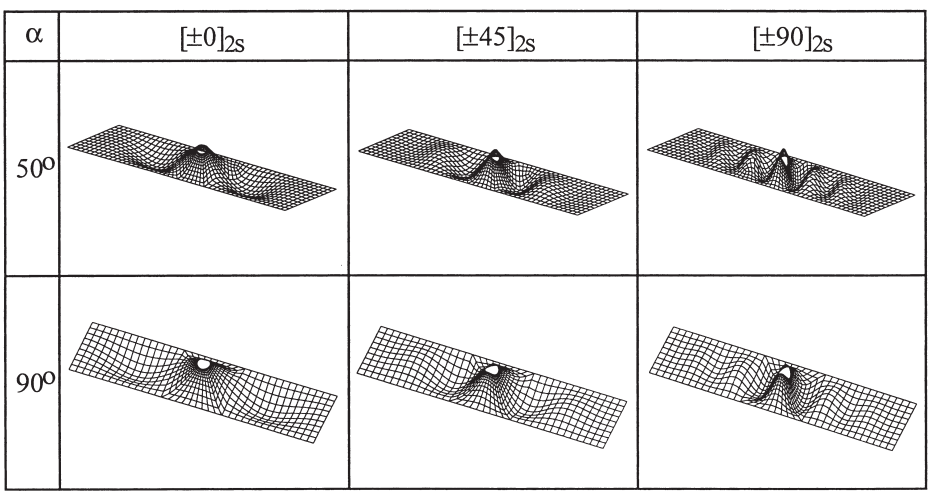

Fig. 18. Buckling modes of clamped composite parallelogram plates with a central circular cutout (d/b=0.2) and with $[\pm 0]_{2S}$, $[\pm 45]_{2S}$ and $[\pm 90]_{2S}$ laminate layups: (a) a/b = 0.5; (b) a/b = 4.

5. Conclusions

For the buckling analysis of uniaxially compressed skew laminated plates with various laminate layups, plate aspect ratios, circular cutouts and end conditions, the following conclusions may be drawn:

1. For composite plates with the same laminate layups and boundary conditions, the buckling loads increase with the decrease of the skew angle α. When the angle

α is smaller, this increase in buckling loads is more prominent. In addition, the buckling modes of plates with small skew angle may have more waves in the loading direction than those of plates with large skew angle and the buckling modes of plates with clamped edges may have more waves than those of plates with simply supported edges.

2. For composite rhombus plates with simply supported edges and with $[90/0]_{2ns}$, $[\alpha/0]_{2ns}$ and $[90/45/0/-45]_{ns}$ laminate layups, the plates with $[90/45/0/-45]_{ns}$ layup usually have the highest buckling loads and the plates with $[\alpha/0]_{2ns}$ layup have the lowest buckling loads. When the edges of plates are all clamped, the $[90/0]_{2ns}$ plates have the highest buckling loads and the $[90/45/0/-45]_{ns}$ plates usually have the lowest buckling loads
3. The highest buckling loads for rhombus $[\pm\theta]_{ns}$ laminate plates usually occur with θ around 45° for simply supported edge conditions and with θ close to 0° for clamped edge conditions. This phenomenon is more consistent when the thickness of the plate is increased.
4. For skew parallelogram $[\pm\theta]_{2s}$ and $[\pm\theta]_{10s}$ laminate short plates (a/b=0.5) with large θ angle, the critical buckling loads generally decrease with the increase of the α angle. However, when the θ angle is close to 0°, the critical buckling loads decrease with the decrease of the α angle. This phenomenon is more prominent for plates with clamped edges than for those with simply supported edges.
5. For skew parallelogram $[\pm\theta]_{2s}$ and $[\pm\theta]_{10s}$ laminate long plates (a/b=4) with simply supported edges, the optimal fiber angle θ usually takes place at 45° for thin plates but shifts to 40° for thick plates. When the edges of plates are changed to clamped conditions, the optimal fiber angle θ still takes place at 45° for thin plates but shifts to 35° for thick plates.
6. For rhombus or parallelogram $[\pm\theta]_{ns}$ plates, the buckling modes of plates with large θ angle tend to have more waves in the loading direction than those of plates with small θ angle.
7. The buckling behaviors of short as well as long skew parallelogram $[\pm\theta]_{2s}$ laminate plates seem not to be significantly influenced by the central circular cutout (except that the buckling loads of the plates are reduced). When the θ angle is large, the plates with cutouts and having a small skew angle α would have large reductions in the critical buckling loads. However, when the θ angle is small, the plates having a small skew angle α would have small reductions in the critical buckling loads. Under the same skew angle α, the same fiber angle θ, the plates with simply supported edges usually have larger reductions in critical buckling loads than those with clamped edges. In addition, the changes of critical buckling loads due to the presence of cutouts for short skew plates are more significant than those for long skew plates. In some cases, the plates with cutouts may have higher critical buckling loads than the same plates without holes.
8. The introduction of cutouts in skew parallelogram laminate long plates may cause the buckling modes of the plates to have fewer numbers of waves in the loading direction than those of plates without cutouts.

References

[1] Crouzet-Pascal J. Buckling analysis of laminated composite plates. Fibre Science and Technology 1978;11:413–46.
[2] Hirano Y. Optimum design of laminated plates under axial compression. AIAA Journal 1979;17:1017–9.
[3] Rhodes MD, Mikulas MM, McGowan PE. Effects of orthotropy and width on the compression strength of graphite–epoxy panels with holes. AIAA Journal 1984;22:1283–92.
[4] Leissa AW. Buckling of laminated composite plates and shell panels. AFWAL-TR-85-3069, Flight Dynamics Laboratory, Air Force Wright Aeronautical Laboratories, Wright–Patterson Air Force Base, Ohio, 1985.
[5] Muc A. Optimal fibre orientation for simply-supported angle-ply plates under biaxial compression. Composite Structures 1988;9:161–72.
[6] Nemeth MP. Buckling behavior of compression-loaded symmetrically laminated angle-ply plates with holes. AIAA Journal 1988;26:330–6.
[7] Hu H-T, Lin B-H. Buckling optimization of symmetrically laminated rectangular plates with various geometry and end conditions. Composite Science and Technology 1995;55:277–85.
[8] Vellaichamy S, Prakash BG, Brun S. Optimum design of cutouts in laminated composite structures. Computers and Structures 1990;37:241–6.
[9] Reddy ARK, Palaninathan R. Buckling of laminated skew plates. Thin-Walled Structures 1995;22:241–59.
[10] Wang CM, Liew KM, Alwis WAM. Buckling of skew plates and corner condition for simply supported edges. Journal of Engineering Mechanics, ASCE 1992;118:651–62.
[11] Morley LSD. Skew Plates and Structures. New York: Macmillan, 1963.
[12] Liao C-L, Lee Z-Y. Elastic stability of skew laminated composite plates subjected to biaxial follower forces. International Journal for Numerical Methods in Engineering 1993;36:1825–47.
[13] Hibbitt, Karlsson, Sorensen, Inc. ABAQUS User and Theory Manuals, Version 5.7, Providence, Rhode Island, 1998.
[14] Chajes A. Principles of Structural Stability Theory. Chapter 1. Englewood Cliffs: Prentice-Hall, 1974.
[15] Cook RD, Malkus DS, Plesha ME. Concepts and Applications of Finite Element Analysis. 3rd ed. New York: John Wiley and Sons, 1989.
[16] Bathe KJ, Wilson EL. Large eigenvalue problems in dynamic analysis. Journal of Engineering Mechanics Division, ASCE 1972;98:1471–85.
[17] Whitney JM. Shear correction factors for orthotropic laminates under static load. Journal of Applied Mechanics 1973;40:302–4.
[18] Tzeng W.-L. Buckling analysis of laminate parallelogram plates subjected to uniaxial compression. Master Thesis, Department of Civil Engineering, National Cheng Kung University, Tainan, R.O.C, 1996.
[19] Crawley EF. The natural modes of graphite/epoxy cantilever plates and shells. Journal of Composite Materials 1979;13:195–205.
[20] Ritchie D, Rhodes J. Buckling and postbuckling behavior of plates with holes. Aeronautical Quarterly 1975;26:281–96.